

Continued obliquity pacing of East Asian summer precipitation after the mid-Pleistocene transition

Li, Tao; Liu, Fei; Abels, Hemmo A.; You, Chen Feng; Zhang, Zeke; Chen, Jun; Ji, Junfeng; Li, Laifeng; Li, Le; Liu, Hou Chun

DOI

[10.1016/j.epsl.2016.09.045](https://doi.org/10.1016/j.epsl.2016.09.045)

Publication date

2017

Document Version

Final published version

Published in

Earth and Planetary Science Letters

Citation (APA)

Li, T., Liu, F., Abels, H. A., You, C. F., Zhang, Z., Chen, J., Ji, J., Li, L., Li, L., Liu, H. C., Ren, C., Xia, R., Zhao, L., Zhang, W., & Li, G. (2017). Continued obliquity pacing of East Asian summer precipitation after the mid-Pleistocene transition. *Earth and Planetary Science Letters*, 457, 181-190. <https://doi.org/10.1016/j.epsl.2016.09.045>

Important note

To cite this publication, please use the final published version (if applicable). Please check the document version above.

Copyright

Other than for strictly personal use, it is not permitted to download, forward or distribute the text or part of it, without the consent of the author(s) and/or copyright holder(s), unless the work is under an open content license such as Creative Commons.

Takedown policy

Please contact us and provide details if you believe this document breaches copyrights. We will remove access to the work immediately and investigate your claim.



Continued obliquity pacing of East Asian summer precipitation after the mid-Pleistocene transition



Tao Li^a, Fei Liu^b, Hemmo A. Abels^c, Chen-Feng You^d, Zeke Zhang^{a,e}, Jun Chen^a, Junfeng Ji^a, Laifeng Li^a, Le Li^a, Hou-Chun Liu^d, Chao Ren^a, Renyuan Xia^a, Liang Zhao^a, Wenfang Zhang^a, Gaojun Li^{a,*}

^a MOE Key Laboratory of Surficial Geochemistry, Department of Earth Sciences, Nanjing University, 163 Xianlindadao, Nanjing 210023, China

^b Earth System Modeling Center and Collaborative Innovation Center on Forecast and Evaluation of Meteorological Disasters, Nanjing University of Information Science and Technology, 219 Ninglu Road, Nanjing 210044, China

^c Department of Geosciences and Engineering, Delft University of Technology, Stevinweg 1, 2628 CN Delft, The Netherlands

^d Earth Dynamic System Research Center, National Cheng Kung University, Tainan 70101, Taiwan

^e Institute of Earth Environment, Chinese Academy of Sciences, Xi'an 710075, China

ARTICLE INFO

Article history:

Received 17 June 2016

Received in revised form 22 September 2016

Accepted 25 September 2016

Available online 26 October 2016

Editor: H. Stoll

Keywords:

microcodium
monsoon dynamics
Milankovitch cycles
climate change
soil carbonate

ABSTRACT

Records from natural archives show that the strength of the East Asian summer monsoon (EASM) strongly depends on the orbital configuration of the Earth. However, the dominant orbital cycles driving EASM have been found to be spatially different. Speleothem stable oxygen isotopic records from southern China, which are believed to reflect large-scale changes in the Asian monsoon system, are dominated by climatic precession cycles. Further north, on the Chinese Loess Plateau (CLP), loess-and-paleosol sequences, which are argued to be controlled by monsoon intensity, are in pace with global ice volume changes dominated by obliquity, and after the mid-Pleistocene transition by 100-kyr cycles. To understand these critical discrepancies, here we apply a novel proxy based on the trace metal compositions of pedogenic carbonate in the eolian deposits on the CLP to reconstruct summer precipitation over the last 1.5 million years. Our reconstructions show that summer precipitation on the CLP is dominantly forced by obliquity not in pace with the ice-volume-imprinted loess-paleosol sequences before and after the mid-Pleistocene transition or with the precession-paced speleothem oxygen isotopic records. Coupled with climate model results, we suggest that the obliquity-driven variations of summer precipitation may originate from the gradient of boreal insolation that modulates the thermal contrast between the Asian continent and surrounding oceans.

© 2016 Elsevier B.V. All rights reserved.

1. Introduction

The East Asian Summer Monsoon (EASM) is an important component of the Asian monsoon system that brings a large amount of moisture to middle and high latitudes of Asian continent and thus influences the livelihood of hundreds of millions of people. Knowledge of how the EASM has evolved in the geological past and understanding the underlying dynamics is crucial to predict its future variability under the very likely scenario of global warming (Wang et al., 2012).

Different proxy archives have suggested very different patterns of orbital scale variation in the EASM (An et al., 2011; Caley et al., 2013; Clemens et al., 2010; Thomas et al., 2014).

On the one hand, the alternations of loess and paleosol layers in the eolian deposits on the Chinese Loess Plateau (CLP), which can be accurately traced by magnetic susceptibility (An et al., 1990), show strong glacial cyclicity (Sun et al., 2006). The paleosol layers with higher magnetic susceptibility are thought to be produced by stronger pedogenesis due to the enhanced precipitation during the interglacial periods compared to the loess layers of glacial periods (Zhou et al., 1990). Other proxies (Chen et al., 1999; Liu et al., 2005) that were used to reflect the intensity of the EASM in eolian deposits on the CLP generally show similar pattern as the magnetic susceptibility that is in pace with global ice volume changes dominated by obliquity, and after the mid-Pleistocene transition by cycles of ~100 thousand years (kyrs). The glacial–interglacial pattern of EASM suggested by the loess-paleosol sequences has also been inferred from lacustrine sediments (An et al., 2011; Ao et al., 2012). Mechanisms proposed for the inferred glacial–interglacial pattern of the EASM include the shifting position of the rainfall

* Corresponding author.

E-mail address: ligaojun@nju.edu.cn (G. Li).

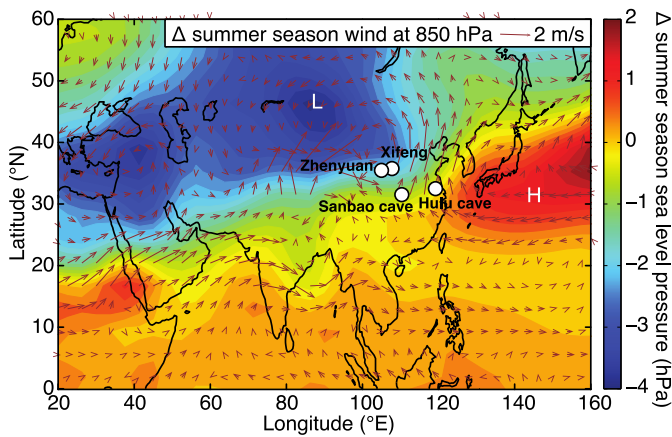


Fig. 1. Model results of summer season sea-level pressure and 850 hPa horizontal wind fields between high and low obliquity. Results denote difference of the 300-yr average results of July, August and September between the 24.5° obliquity run and the 22.1° obliquity run. L and H label the centers of low and high sea-level pressure of the present average summer climatology. Also labeled are study sites on the CLP and the Sanbao and Hulu cave.

belt or the exposure of the continental shelf in response sea-level lowering caused by increasing Northern Hemisphere ice volume (Liu and Ding, 1998), bi-hemispheric forcing (An et al., 2011; Caley et al., 2013), and influence of the atmospheric CO₂ concentration (Lu et al., 2013).

The inferred glacial–interglacial pattern of the EASM, however, has been challenged by the cave deposits in southern China, whose stable oxygen isotopic compositions reveal a dominance of climatic precession cycles of ~23 kyrs (Cheng et al., 2009; Cheng et al., 2016; Wang et al., 2008). Though highly debated, it is generally accepted that the speleothem $\delta^{18}\text{O}$ records in southern China reflect large-scale changes of Asian monsoon (Cheng et al., 2016). The dominance of precession cycles in speleothem $\delta^{18}\text{O}$ has also been seen in other records from tropical monsoon systems globally (Cheng et al., 2012), which collectively suggests that low latitude insolation and thus the inter-tropical convergence zone (ITCZ) regulates the intensity of monsoonal circulation (Cheng et al., 2012; Yancheva et al., 2007).

It has been suggested that the discrepancies between loess-paleosol sequences and the speleothem oxygen isotopic records may reflect the possible spatial difference on the orbital forcing of summer monsoon intensity (Ao et al., 2012). However, the CLP is only ~500 km north of the Sanbao cave (Fig. 1), where most of the long-term speleothem records were generated (Cheng et al., 2009, 2016; Wang et al., 2008). It is very unlikely that the EASM, a large-scale climatic system, behaves differently within such a short distance. Instead, the discrepancies between the loess and speleothem records may reflect the fact that most of the current proxies are measures of more processes than the intensity of the EASM alone.

In the loess records, a key factor that changes considerably during glacial–interglacial cyclicity is the strength of the winter monsoon (An et al., 1991). During interglacial periods, a weaker winter monsoon brings less and finer dust to the CLP, which consequently lowers depositional rates to about a quarter of the rates during glacial dust deposition. A lowered rate of deposition increases the time available for pedogenesis. The coincident smaller grain sizes of the transported dust (Prins et al., 2007) increases the reactive surface for pedogenic alteration and lowers the permeability of the soils, so that less water is needed for soil formation. In addition to the weaker winter monsoon bringing less and finer dust, higher temperature and $p\text{CO}_2$ (Petit et al., 1999) during interglacial stages may also have contributed to the stronger pedogenesis of paleosol

layers through the kinetics of chemical weathering and biotic activities.

In the cave archives, considerable debate remains on interpretation of the speleothem $\delta^{18}\text{O}$ records. The amount effect was initially employed to establish the link between the strength of the Asian monsoon and the speleothem $\delta^{18}\text{O}$ records (Yuan et al., 2004). As demonstrated by several studies (e.g. Liu et al., 2014; Cheng et al., 2009; Clemens et al., 2010), the amount effect caused by local summer precipitation amount can hardly explain the $\delta^{18}\text{O}$ of rainwater in the cave sites. It is more likely that the upstream processes exert stronger control on speleothem $\delta^{18}\text{O}$ than local precipitation amount (Caley et al., 2014; Liu et al., 2014). Changing precipitation seasonality and moisture sources may also contribute to the speleothem $\delta^{18}\text{O}$ signals (Clemens et al., 2010; Maher and Thompson, 2012; Orland et al., 2015). Nevertheless, all of these influencing factors favor the interpretation of $\delta^{18}\text{O}$ as a reflection of the hydrologic processes and circulation regime over a large part of the Indo–Asian region but not necessarily the strength of the EASM.

Quantitative reconstruction of summer precipitation in East Asia is critical to solve the puzzle regarding the variation of the EASM. Records of the EASM in the geological archives have sought to reconstruct the amount of precipitation since other monsoon characteristics, such as the velocity of southerly winds, are not typically preserved in the sedimentary archives. The best place of such record is in northern China (Chen et al., 2015; Rao et al., 2016), where the precipitation amount is principally controlled by the strength of the EASM (Ding et al., 2008).

A new method has been developed recently to reconstruct intensity of precipitation based on the incorporation of trace metals into microcodium, which is a very pure, pedogenic form of carbonate that precipitates in eolian deposits on the CLP (Li and Li, 2014). The amount of strontium and magnesium incorporated into microcodium from the soil solution is determined by local precipitation (Li and Li, 2014). Lower intensity and frequency of precipitation results in a higher proportion of calcium extracted from the soil solution by the precipitation of secondary carbonates (Li and Li, 2014). This leaves the soil solution with higher strontium to calcium ratio (Sr/Ca) and magnesium to calcium ratio (Mg/Ca) due to the low partition coefficients ($\ll 1$) of strontium and magnesium in calcite. Lower precipitation therefore results in higher Sr/Ca and Mg/Ca ratios stored in microcodium (Li and Li, 2014). Thus, Sr/Ca and Mg/Ca ratios of microcodium can be used to reconstruct precipitation quantitatively.

In this study, we first show that microcodium Mg/Ca ratio is less suitable as a precipitation proxy because of its potential dependence on temperature, calcification rate, and composition of the original soil solution. Oxygen isotopic compositions of microcodium collected from Holocene soils suggest that microcodium is more likely to be formed during summer monsoon seasons. We then establish a 1500-kyr-long summer precipitation record on the CLP based on the Sr/Ca ratios of microcodium with updated calibration equation. Two parallel reconstructions covering the last 500 thousand years are performed to test the reliability of microcodium Sr/Ca proxy as a regional measure of summer precipitation. Moreover, sensitivity experiments forced by variations of orbital parameters are conducted using a general circulation model of intermediate complexity to test the sensitivity of the EASM to orbital forcing. Coupling our geochemical records with model results, we highlight the underestimated role of obliquity in regulating the EASM variability.

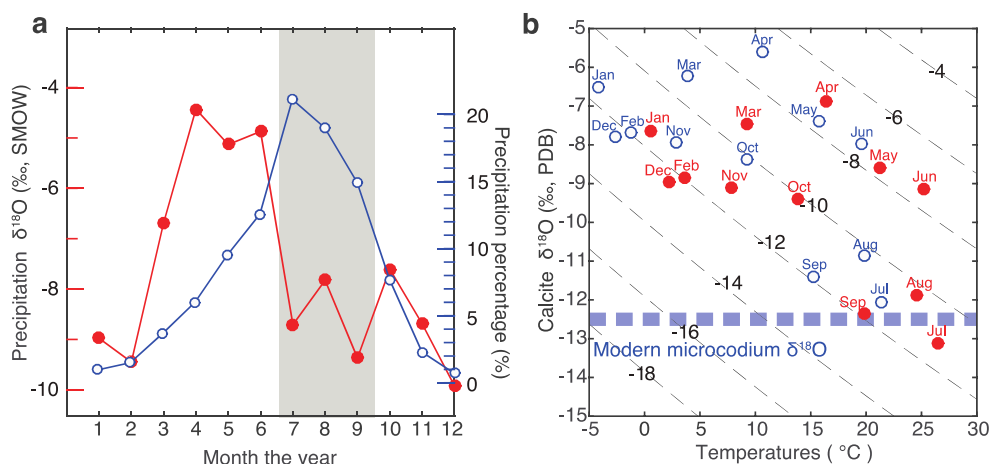


Fig. 2. The seasonality of the microcodium records. (a) Present-day percentage of monthly precipitation (blue open cycles) and rainwater $\delta^{18}\text{O}$ (red solid cycles) on the Chinese Loess Plateau. The shaded bar indicates the summer monsoon season. (b) Calculated oxygen isotopic composition of calcite precipitated in deferent months based on averaged daily highest temperatures (red solid cycles) and averaged daily mean temperatures (blue open cycles) compared with that of the microcodium in modern soil (thick dash line) in Xifeng site. Black dash lines show contours of different rainwater $\delta^{18}\text{O}$ (relative to SMOW, ‰). The rainwater $\delta^{18}\text{O}$ data are from the Global Network of Isotopes in Precipitation (GNIP) database at http://www-naweb.iaea.org/napc/ih/IHS_resources_gnip.html. (For interpretation of the references to color in this figure, the reader is referred to the web version of this article.)

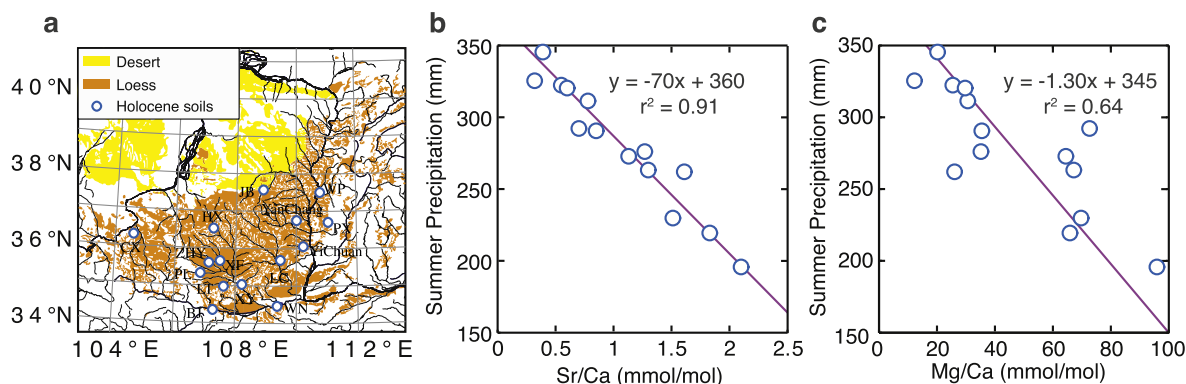


Fig. 3. Proxy calibration. (a) Map showing the location of the Holocene soils used in the calibration. (b) and (c) Correlation between local summer precipitation (July, August and September) and the Sr/Ca and Mg/Ca ratios of microcodium in Holocene soils.

2. Methods

2.1. Samples and measurements

The CLP (Fig. 1) receives about 70% of its annual rainfall during the summer (July to September; Fig. 2a), a typical monsoon-influenced region (Wang et al., 2012). The eolian deposits on the CLP are well-dated back to the late Oligocene by magnetic stratigraphy (Guo et al., 2002; Sun et al., 1998). The Quaternary eolian deposits consist of a regular alternation of loess and paleosol layers that correspond to glacial–interglacial climate changes (Liu and Ding, 1998). Samples of Holocene soils were taken from six new sites as well as the sites that were employed to calibrate the transfer function in our previous study (Fig. 3a; Supplementary Table 1) (Li and Li, 2014). The samples that were used to reconstruct precipitation were taken from the Xifeng (107°47'E, 35°45'N) and Zhenyuan sections (107°12'E, 35°43'N) on the central CLP (Fig. 1). The depth resolution of the samples was 5 cm, which is equivalent to time resolution of ~500 yrs. The Xifeng and Zhenyuan sections can be well correlated to each other using magnetic susceptibility stratigraphy (Fig. 6a, b).

Magnetic susceptibility of the loess samples were measured using a Bartington MS2 meter at the MOE Key Laboratory of Surficial Geochemistry, Nanjing University. About 20 pieces of microcodium were picked from the sieved (>75 μm) loess sample

under binoscope by hand according to its diagnostic transparent white color and cell-like structure (Supplementary Fig. 1a). Observation under scanning electron microscope shows that the cell-like structure of microcodium is well preserved throughout the profile (Supplementary Fig. 1b–f), indicating limited diagenetic alteration. The Sr/Ca and Mg/Ca ratios of the picked microcodium were then measured according to the method of Li and Li (2014). The long-term precision of measured Mg/Ca and Sr/Ca ratios are better than 5% and 3%, respectively. Stable and radiogenic strontium isotopes of the microcodium in Holocene soils and randomly-selected samples from the Xifeng profile were measured following the method of Liu et al. (2012) at the Isotope Geochemistry Laboratory, National Cheng Kung University, Taiwan. The composition of stable strontium isotopes was expressed as $\delta^{88/86}\text{Sr}$ relative to NBS987 (Liu et al., 2012). The external reproducibility of $\delta^{88/86}\text{Sr}$ value and $^{87}\text{Sr}/^{86}\text{Sr}$ ratio during experiments for international seawater standard IAPSO is better than 0.03‰ and 0.000014, respectively (2σ , $n = 7$). The oxygen isotopes of the picked microcodium from modern soils at the Xifeng site were measured using a MAT-253 gas-sourced mass spectrometry coupled with a Kiel IV carbonate device at Nanjing Institute of Geology and Palaeontology, Chinese Academy of Sciences (CAS). $\delta^{18}\text{O}$ values are reported relative to PDB with a precision of $\pm 0.16\text{‰}$ (2σ).

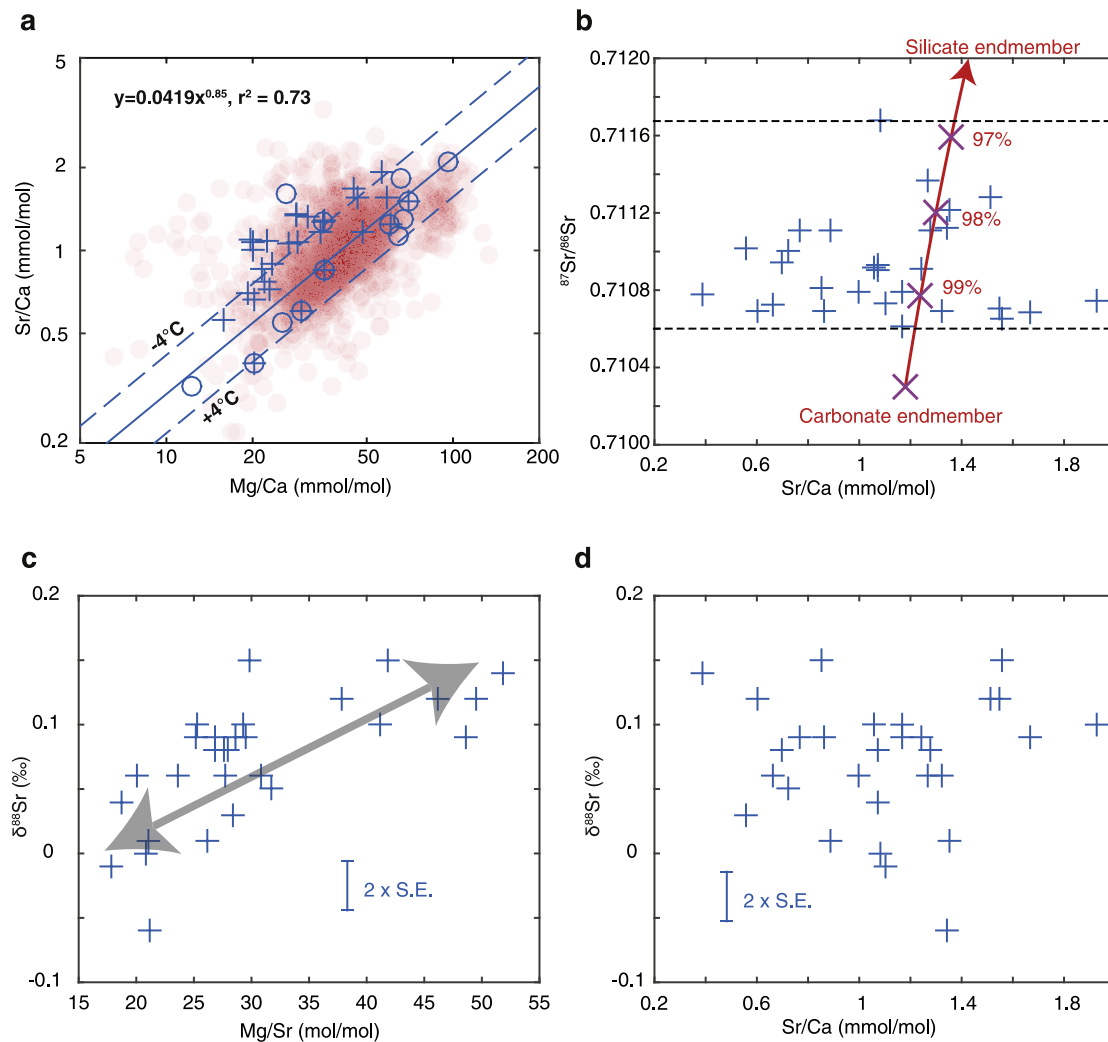


Fig. 4. Geochemical constraints on the advantages of Sr/Ca ratio over the Mg/Ca ratio. (a) Correlation between the Mg/Ca and Sr/Ca ratios of microcodium. The red filled circles of 10% opacity are all samples in this study. Blue open circles are samples of Holocene soil used in the calibration. Crosses are samples used to measure stable and radiogenic strontium isotopes. Solid line shows the best correlation and dash lines illustrate the shifting correlation due to the influence of temperature on the incorporation of Mg in calcite. (b) The Sr/Ca ratios of original soil solutions constrained by microcodium $^{87}\text{Sr}/^{86}\text{Sr}$ ratios. (c) and (d) Correlation between stable strontium isotopes and Mg/Sr and Sr/Ca ratios of microcodium. (For interpretation of the references to color in this figure, the reader is referred to the web version of this article.)

2.2. Age model, stack and wavelet analysis

The age model is constructed by correlating grain size of the loess and paleosol to global ice volume. It has been generally accepted that the grain size of the eolian deposits on CLP reflects the strength of winter monsoon (An et al., 1991), which is closely linked to the strength of the Siberian High pressure cell and, with that, to ice volume (Ding et al., 1995; Hao et al., 2012). The tie points of the age model are based on the rapid shifts in grain size, which mostly correspond to glacial terminations approximated by the $\delta^{18}\text{O}$ of benthic foraminifera (Lisiecki and Raymo, 2005) (Fig. 5, Supplementary Table 3). The age between the tie-points is interpolated linearly. The resulting age model (Fig. 5) is very similar to the ones obtained by orbital tuning for other CLP series (Sun et al., 2006) and is consistent with recent constraints on the Brunhes–Matuyama magnetic polarity reversal (Zhou et al., 2014).

Precipitation data is stacked by a Gaussian filter with standard deviation of the Gaussian window of 0.5 kyr. The time series used in the wavelet analysis are linear interpolations in step of one thousand years. Morlet wavelets are used in the analysis (Torrence and Compo, 1998). Both red and white noise backgrounds are considered to estimate the confidence levels (Torrence and Compo,

1998). Wavelet coherence is applied to exam the coherence and phase relationship of the coherence between different time series (Grinsted et al., 2004). The red noise backgrounds are assessed using Monte Carlo methods to yield statistical significance (Grinsted et al., 2004).

2.3. Climate model

Two obliquity experiments with the Community Earth System Model version 1 (CESM1) were analyzed: a 300-yr run with a high (24.5°) obliquity and a 300-yr run with a low (22.1°) obliquity. CESM1 is Earth System Model that was developed by the National Center for Atmospheric Research (NCAR) in July 2010 as a freely available global climate model for the wider climate research community at its website (<http://www.cesm.ucar.edu/models/cesm1.0/>). It is a fully coupled, community, global climate model, which is composed of five separate model components simultaneously simulating the Earth's atmosphere, ocean, land, land-ice, and sea-ice, plus one central coupler.

A lower resolution version of the CESM1 was run here. Atmospheric model is the Community Atmosphere Model (CAM4) with T31 horizontal resolution (about $3.75^\circ \times 3.75^\circ$) and 26 layers in

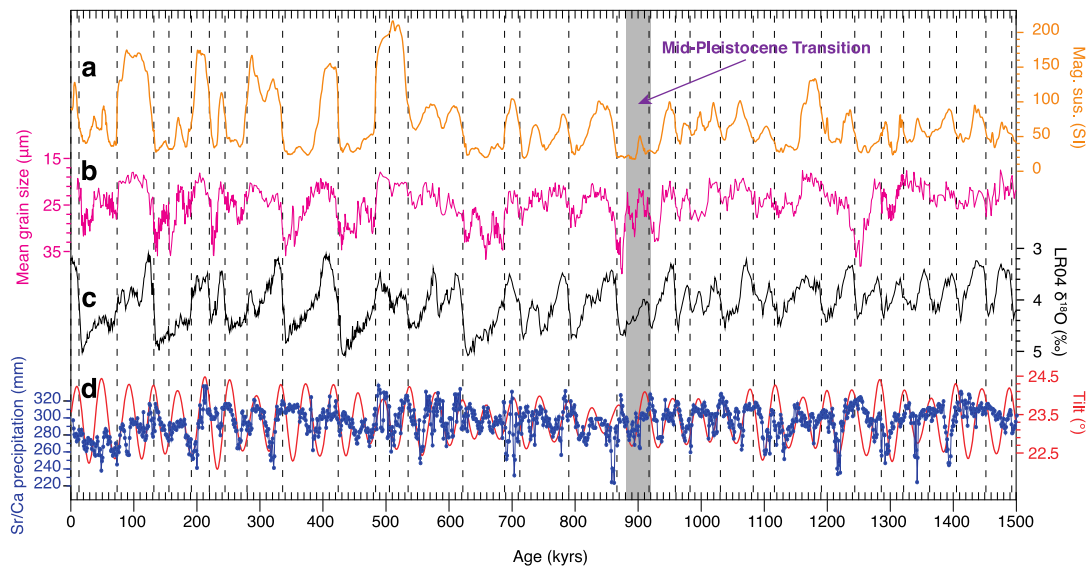


Fig. 5. Reconstructed Sr/Ca summer precipitation on the Chinese Loess Plateau over the past 1500 thousand years at Xifeng. (a) and (b) Magnetic susceptibility and mean grain size of Xifeng section (Sun et al., 2006). (c) LR04 benthic $\delta^{18}\text{O}$ (Lisiecki and Raymo, 2005). (d) Reconstructed Sr/Ca summer precipitation at Xifeng compared with Earth's obliquity (Berger and Loutre, 1991). Shade bar indicates the mid-Pleistocene transition at ~ 900 ka (Elderfield et al., 2012).

the vertical. Land model is the Community Land Model (CLM4), which adopts the same horizontal resolution as the CAM4. The ocean model is based on the Parallel Ocean Program (POP) version 2 with 100 latitudinal grids, 116 longitudinal grids, and 60 vertical layers. An initial forced integration of 200 yrs was performed to reach the equilibrium simulations. The two obliquity experiments are simulated based on the 2000-yr control run with constant CO_2 (284.7 ppm), N_2O (275.68 ppb), and CH_4 (791.6 ppb), and fixed ice volume, incoming solar radiation at the top of the atmosphere (1360.9 W m^{-2}) as described in Rosenbloom et al. (2013).

3. Results

The Sr/Ca ratios of microcodium in the 15 Holocene soil profiles show good correlation ($r^2 = 0.91$) with the amounts of modern summer (July, August and September) precipitations (Fig. 3b; Supplementary Table 1). However, the correlation between the Mg/Ca ratios of microcodium and summer precipitation is more scattered ($r^2 = 0.64$) (Fig. 3c). The correlation between the Mg/Ca and Sr/Ca ratios also shows a scattered pattern along the positive correlation line predicted by the Rayleigh fractionation model ($r^2 = 0.73$) (Fig. 4a) (Li and Li, 2014). Small variations between 0.7106 and 0.7117 have been observed for the $^{87}\text{Sr}/^{86}\text{Sr}$ ratios of microcodium (Fig. 4b). Detectable changes between -0.1‰ to 0.15‰ can be found for the stable strontium isotopic compositions ($\delta^{88/86}\text{Sr}$) of microcodium, which correlate positively with the Mg/Sr ratios instead of Sr/Ca ratios (Fig. 4c, d). The $\delta^{18}\text{O}$ values of Holocene microcodium from Xifeng site are characterized by narrow range with an average value of $-12.5\text{‰} \pm 0.5\text{‰}$ (2σ , $n = 7$) (Fig. 2b).

The reconstructed summer precipitation at Xifeng and Zhenyuan sections varies from ~ 200 mm to ~ 320 mm over the last 1.5 million years (Fig. 5d; Fig. 6e, f), which is within the range of the Holocene calibration (Fig. 3b). The two parallel sections, which are correlated stratigraphically by magnetic susceptibility (Fig. 6a, b), show consistent patterns of summer precipitation records over the past 480 kyr (Fig. 6e, f). The precipitation record shows a persistent obliquity cycle of the 41-kyr over the last 1500 kyr, including the period after the mid-Pleistocene transition (MPT) at ~ 900 kyr ago (Elderfield et al., 2012) (Fig. 5). No post-MPT glacial cycles of ~ 100 kyrs and precession cycle of ~ 23 kyrs can be detected at 95% confidence level (Fig. 7a). High summer precip-

itation on the Chinese Loess Plateau (CLP) is generally associated with high obliquity (Fig. 5; Fig. 6; Fig. 8d).

4. Discussion

4.1. Advantages of Sr/Ca ratio over the Mg/Ca ratio

The scattered correlations of microcodium Mg/Ca ratio to the amount of precipitation (Fig. 3c) and to the Sr/Ca ratio (Fig. 4a) may reflect the complexities associated with the incorporation of magnesium into calcite, which may be related to variations in temperature, calcification rate, and the composition of the original soil solution.

Relative constant Sr/Ca and Mg/Ca ratios for the initial weathering product are required when applying microcodium Sr/Ca and Mg/Ca ratios as proxies for rainfall (Li and Li, 2014). However, the content of dolomite in loess and paleosol changes dramatically (Li et al., 2007a), which may influence the Mg/Ca ratios of the initial weathering products. On average, dolomite and calcite in loess deposits have similar Sr/Ca ratios. A simple binary mixing model between silicate weathering and carbonate weathering end-members can be used to assess the influences of changes in initial weathering products on Sr/Ca ratios (Fig. 4b). The silicate end-member has a higher Sr/Ca ratio of 7.14 mmol/mol (Chen et al., 2007) and a more radiogenic $^{87}\text{Sr}/^{86}\text{Sr}$ ratio of 0.7185 (Li et al., 2009), while the detrital carbonate is characterized by a lower Sr/Ca ratio of ~ 1.18 mol/mol and a less radiogenic $^{87}\text{Sr}/^{86}\text{Sr}$ ratio of 0.7103 (Rao et al., 2009). Carbonate weathering contributes $>97\%$ to the Ca found in soil solutions (Fig. 4b). The small variation in the $^{87}\text{Sr}/^{86}\text{Sr}$ ratios of microcodium points to a relatively stable source of the strontium, and thus a stable Sr/Ca ratio in the initial weathering product (Fig. 4b).

The partition coefficient of Mg between solution and calcite is a strong function of temperature (Elderfield and Ganssen, 2000). Magnesium is more easily incorporated into calcite at higher temperatures. A glacial–interglacial temperature change of $\sim 8^\circ\text{C}$, as shown by the Δ_{47} clumped-isotope data (Eagle et al., 2013) and brGDGTs-derived air temperatures (Peterse et al., 2014), can explain most of the scattering associated with the correlation between Mg/Ca and Sr/Ca ratios (Fig. 4a), taking into account a temperature dependence of $\sim 10\%$ per $^\circ\text{C}$ for partition coefficient of Mg

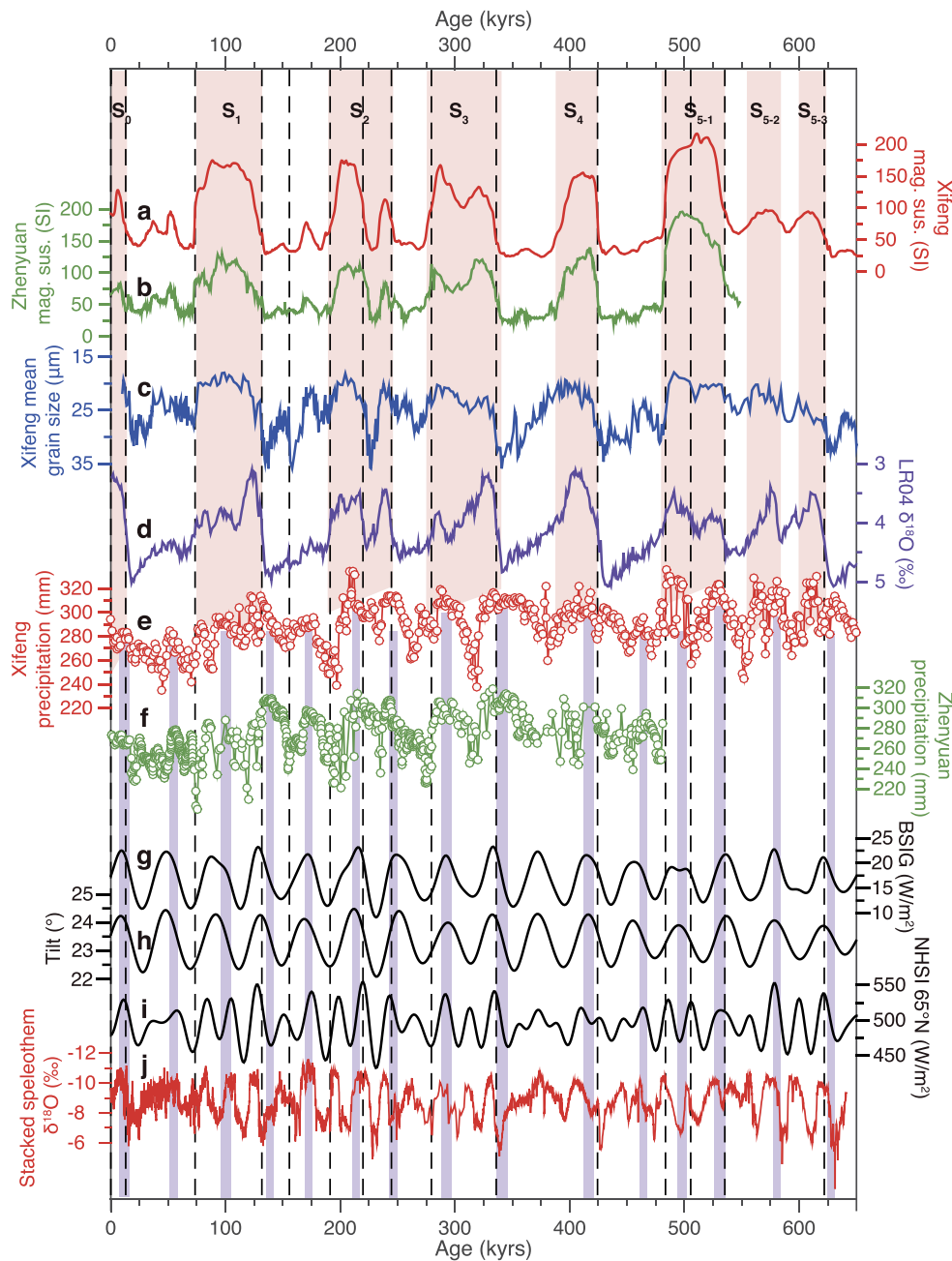


Fig. 6. Comparison of summer precipitation on the Chinese Loess Plateau with other records over the past 650 thousand years. (a) and (b) Magnetic susceptibility of Xifeng and Zhenyuan section (Sun et al., 2006). (c) Mean grain size of Xifeng section (Sun et al., 2006). (d) LR04 benthic $\delta^{18}\text{O}$ stack (Lisiecki and Raymo, 2005). (e) and (f) Reconstructed summer precipitation at Xifeng and Zhenyuan sites (open circles are smoothed record with a 0.5-ky Gaussian filter). (g) Boreal summer insolation gradient (BSIG) between 25°N and 45°N (Berger and Loutre, 1991). (h) Earth's obliquity (Berger and Loutre, 1991). (i) Northern hemisphere summer insolation (NHSl) at 65°N (Berger and Loutre, 1991). (j) Asian speleothem $\delta^{18}\text{O}$ stack (Cheng et al., 2009; Cheng et al., 2016; Wang et al., 2008). Light purple bars show positions of high summer precipitation that is correlated with high obliquity. Vertical red bars indicate the paleosol layers. (For interpretation of the references to color in this figure, the reader is referred to the web version of this article.)

in calcite (Elderfield and Ganssen, 2000). Such glacial–interglacial temperature changes can change the Mg/Ca ratios of calcite by a factor of ~ 2 , or more than half of the changes in the observed Mg/Ca ratios of microcodium. Conversely, the incorporation of strontium into calcite is not very temperature-sensitive (Tang et al., 2008) when compared with the large variation (up to a factor of 4) in the Sr/Ca ratios of microcodium.

An indicator of the impact of temperature on the incorporation of magnesium into microcodium may come from the positive correlation between the Mg/Sr ratios and the $\delta^{88/86}\text{Sr}$ values (Fig. 4c). The Mg/Sr ratio is used to approximate the partition coefficient of magnesium as its normalization to strontium can eliminate the ef-

fect of Rayleigh fractionation on the Mg/Ca ratios of soil solutions (Li and Li, 2014). A previous study has shown that the light strontium isotope (^{86}Sr) is preferentially incorporated into calcite at ambient conditions (Böhm et al., 2012). Like other isotopic systems, the kinetic fractionation of stable strontium isotopes between calcite and solution is lesser at higher temperatures (Fietzke and Eisenhauer, 2006), which results in higher $\delta^{88/86}\text{Sr}$ values in the calcite. Instead, no correlation could be found between the Sr/Ca ratios and the $\delta^{88/86}\text{Sr}$ values of microcodium (Fig. 4c), which is consistent with the relatively weak dependence of strontium incorporation into calcite on temperatures (Tang et al., 2008).

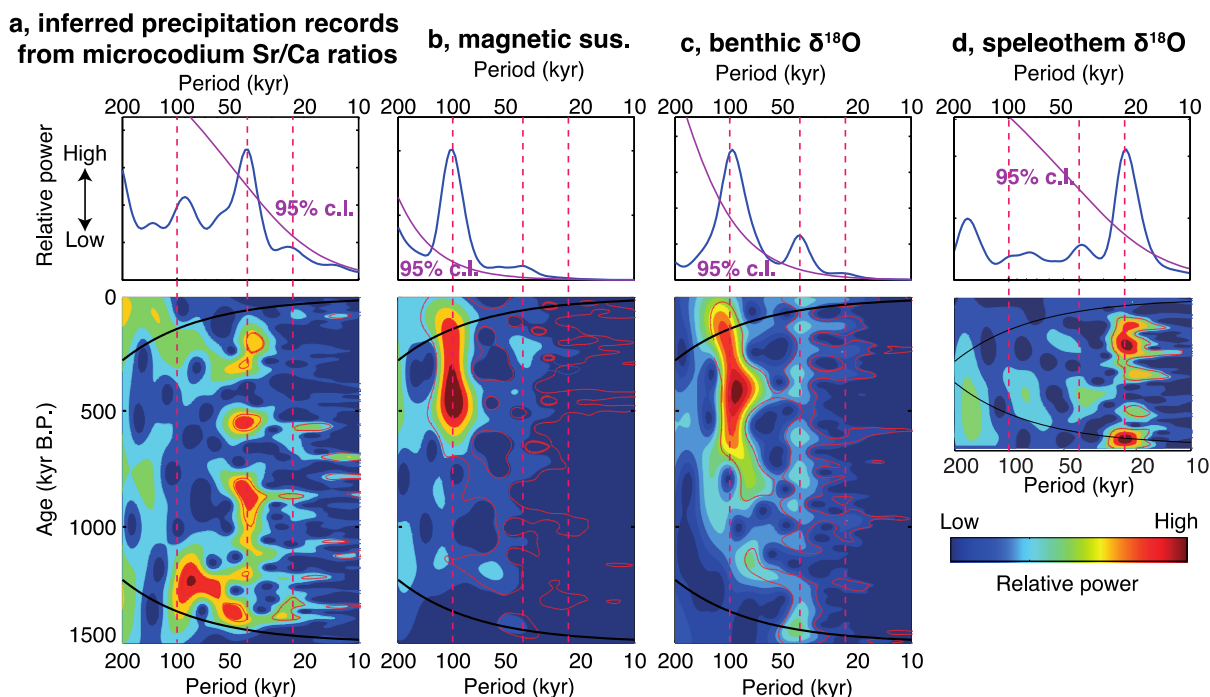


Fig. 7. Wavelet analysis for (a) the reconstructed summer precipitation and (b) magnetic susceptibility of the eolian deposits on the Chinese Loess Plateau (Sun et al., 2006), (c) LR04 composite of benthic $\delta^{18}\text{O}$ (Lisiecki and Raymo, 2005), and (d) speleothem $\delta^{18}\text{O}$ (Cheng et al., 2009; Cheng et al., 2016; Wang et al., 2008). The blue curves in the upper panels are global spectrum with purple lines showing the 95% confidence level. The lower panels are the corresponding evolving spectrum power through time, with the enclosed purple curve showing the regions with >95% confidence level. The dashed line indicates the periodicities of 100 kyr, 41 kyr, and 23 kyr, respectively. (For interpretation of the references to color in this figure, the reader is referred to the web version of this article.)

The incorporation of magnesium into calcite is also a strong function of crystal growth rate (Mavromatis et al., 2013). However, a higher growth rate would result in a higher $\delta^{88/86}\text{Sr}$ value (Böhm et al., 2012) and lower magnesium partition coefficient (Mavromatis et al., 2013), which is opposite to the observed positive correlation between the $\delta^{88/86}\text{Sr}$ values and the Mg/Sr ratios (Fig. 4c). Nevertheless, the incorporation of strontium into calcite is much less sensitive to the growth rate compared to magnesium (Fig. 4d) (Mavromatis et al., 2013; Tang et al., 2008), supporting the reliability of Sr/Ca ratio as a record of soil solution composition.

4.2. Microcodium Sr/Ca ratio as proxy for summer precipitation

Pedogenic carbonates can record summer precipitation only if they are precipitated during summer seasons. Clumped-isotope thermometry shows that soil carbonates on the Chinese Loess Plateau (CLP) are most likely precipitated during summer (Eagle et al., 2013), which is consistent with other soil carbonate worldwide (Quade et al., 2013). Using the fractionation function at low temperatures (Kim and O'Neil, 1997), where $1000 \ln \alpha = 18.03 (103T - 1) - 32.42$ (α is the fractionation factor), the soil temperature, and the average $\delta^{18}\text{O}$ of rainwater, we can calculate the theoretical $\delta^{18}\text{O}$ values of the calcite precipitated in ambient environments (Fig. 2b). The monthly precipitation weighted average $\delta^{18}\text{O}$ of rainwater is taken from Xi'an site, ~190 km southeast of the Xifeng site, because rainwater data of Xifeng site is unavailable. An appropriate shift by -2.45‰ has been made to account for the difference of the two sites according to the difference of precipitation-weighted rainwater $\delta^{18}\text{O}$ between Xi'an and Pingliang because Pingliang has a similar distance downwind of Xi'an as Xifeng (Zhang and Yao, 1998). Monthly average daily maximum air temperature is used for shallow soil temperature because the soil carbonate is likely precipitated under daily maximal temperatures that occur in the early afternoon (Quade et al., 2013). The results suggest that the very low $\delta^{18}\text{O}$ value of the Holocene mi-

crocodium (-12.5‰ , $n = 7$), which is much lower than other types of authigenic carbonate in the loess sequences (Li et al., 2007b; Sheng et al., 2008), only matches with the low $\delta^{18}\text{O}$ value of calcite that precipitates during the summer monsoon season (Fig. 2b). Using monthly daily average temperature would result in higher $\delta^{18}\text{O}$ value of the precipitated calcite that will not match the low $\delta^{18}\text{O}$ of microcodium (Fig. 2b). Thus, we argue that microcodium is precipitated during the summer season and can therefore record trace metal compositions of soil solution in that season.

The good correlation between Sr/Ca ratios of microcodium and amounts of summer precipitation (P ; Fig. 3b) allows to reconstruct summer precipitation via $P = -70 \times \text{Sr/Ca} + 360$ ($r^2 = 0.91$). The relative error of reconstructed summer precipitation is about ± 3 mm given that the precision of Sr/Ca measurements is better than 0.04 (2σ). Absolute error in precipitation calculations may be larger, because, for the calibration, summer precipitation in Holocene soils is based on modern observations. Climate change during the course of the Holocene gradually lowered precipitation towards the recent (An et al., 2000; Wang et al., 2005). Too low estimation of average Holocene precipitation in the calibration of the Sr/Ca precipitation proxy will result in underestimation of paleo-precipitation reconstructions. But, as the whole set of calibrated soils will likely underestimate of summer precipitation for the Holocene, this will influence the absolute numbers rather than the observed patterns over time.

The similarity of the Sr/Ca patterns between Xifeng and Zhenyuan section (Fig. 6e, f) proves that the Sr/Ca proxy likely reproduces a signal that is related to summer precipitation instead of other local factors. Small differences between the two sections might be attributed to local precipitation differences or to the poor correlation between the sites caused by small-scale diachroneity of magnetic susceptibility changes or variable sedimentation rates in a certain layer.

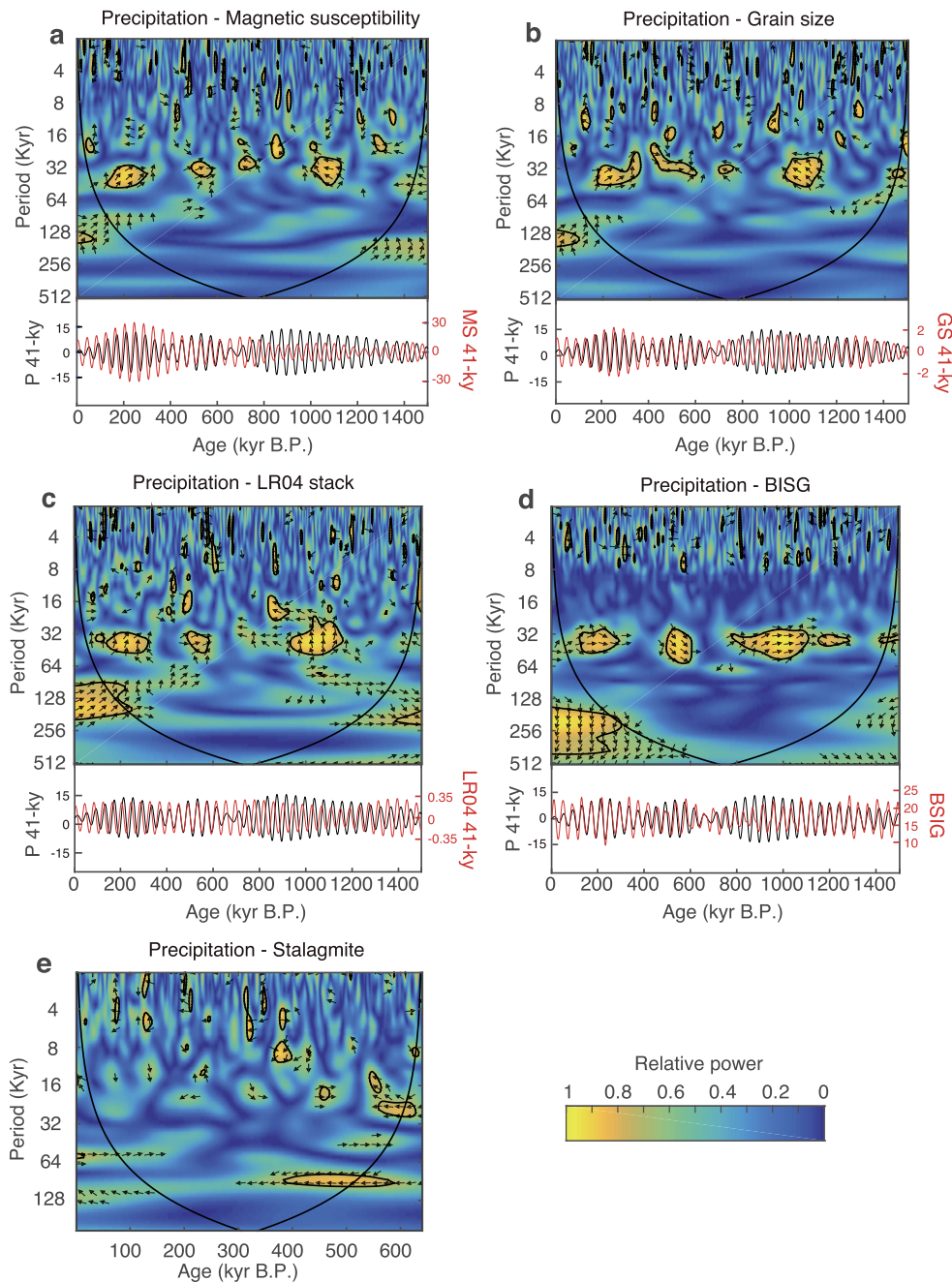


Fig. 8. Wavelet coherences between microcodium Sr/Ca based summer precipitation record and (a) magnetic susceptibility (Sun et al., 2006), (b) mean grain size (Sun et al., 2006), (c) ice volume (Lisiecki and Raymo, 2005), (d) boreal summer insolation gradient (BSIG) (Berger and Loutre, 1991), and (e) speleothem $\delta^{18}\text{O}$ record (Cheng et al., 2009, 2016; Wang et al., 2008). Thick contours show the 95% confidence level. Arrows illustrate the relative phase relationship, with right arrow indicating in-phase, left arrow indicating anti-phase, and upward arrow indicating leading of summer precipitation by 90° . Lower panels of (a)–(d) show the comparison of summer precipitation record with other records at 41-ky band using band-pass filter with central frequency of 0.0244 and bandwidth of 0.003.

4.3. Obliquity pacing of summer precipitation

The dominance of obliquity-driven variability in summer precipitation is very different from the intensity of pedogenesis reflected by the alternation of loess and paleosol layers at the same sites (Fig. 5; Fig. 6; Fig. 7; Fig. 8). Although they both show significant power at obliquity band (Fig. 7a, b, e, f; Fig. 8a), the strong glacial cyclicity visible in loess-paleosol alternations represented by magnetic susceptibility (Sun et al., 2006) is at ~ 100 kyrs pacing after the mid-Pleistocene transition (Fig. 7b). Whether or not the 100-kyr glacial-interglacial cycles are driven by obliquity or eccentricity (Huybers and Tziperman, 2008), the patterns are very different from the Sr/Ca summer precipitation records at the ex-

act same sites. This argues that most of the current proxies that trace the loess-and-paleosol alternations is influenced by other processes than the EASM. The factors that could possibly contribute to the signal of glacial cycles in these proxies include the depositional rate, grain size, temperature, and $p\text{CO}_2$.

The reconstructed summer precipitation on the CLP also shows some precession-related variability, but it seems to be different from the dominant ~ 23 -kyrs precession-forced periodicity seen in speleothem $\delta^{18}\text{O}$ records in southern China (Fig. 6j; Fig. 7d; Fig. 8e). The different evolution between the amount and the $\delta^{18}\text{O}$ of precipitation has also been recorded in lacustrine sediments in North China (Rao et al., 2016). A recent study based on leaf wax in loess even shows different pattern of rainwater $\delta^{18}\text{O}$ (inferred from

$\delta^2\text{H}$) compared to the speleothem records, which argues complexity associated with oceanic and continental vapor source due to the latitudinal gradients in the influence of the winter and summer monsoons (Thomas et al., 2016). Nevertheless, the entirely absence of obliquity cycles in speleothem $\delta^{18}\text{O}$ records and the strong obliquity signal in Sr/Ca-precipitation proxy may suggest that speleothem $\delta^{18}\text{O}$ records largely reflect the hydrological processes occurred at tropical regions (Caley et al., 2014; Liu et al., 2014), which is fundamentally governed by the precession-paced insolation change instead of obliquity induced forcing that control the strength of the EASM.

We propose that the obliquity forcing of summer precipitation on the CLP originates from the gradient of boreal summer insolation (Fig. 6g). The influence of obliquity on summer insolation is stronger in high latitudes than in low latitudes. Instead, precession has similar influence on the insolation of different latitudes. Thus, the gradient of boreal summer insolation is dominated by the 41-kyr obliquity signal with an insignificant precession component (Raymo et al., 2006) (Fig. 6g). Unlike most tropical monsoon systems, the East Asian summer monsoon (EASM) extends as far as 50°N (Wang et al., 2012), possibly due to the extensive low-pressure system associated with the massive Asian continent (Fig. 1). Modern observations show that precipitation in the northern monsoon regions of East Asia is controlled by the strength of the moisture-bearing southerly winds (Ding et al., 2008). A higher gradient of boreal summer insolation may introduce a greater contrast between the low-pressure system over the high-latitude continental landmass and the high-pressure system over the ocean in relatively lower latitudes, and thus stronger southerly winds.

We test this mechanism by conducting sensitivity experiments using a general circulation model under obliquity maximum (24.5°) and minimum (22.1°) conditions (Fig. 1). Difference of summer climatology, which is represented by sea-level pressure and 850 hPa horizontal wind fields, is calculated from the 300-yr average of July, August and September between the high and low obliquity runs (24.5° run minus the 22.1° run). Sea-level pressure decreases by about 4 hPa in the center of Asian continents and increases by up to 2 hPa in the mid-latitude Pacific Ocean during obliquity maxima. This results in about a 50% increase in the pressure contrast between the landmass and ocean. Consequently, the southerly winds increase by about 2 m/s in East China, which almost double the present-day value.

The response of summer precipitation to obliquity in the modeling is more complex, possibly due to the large error associated with the relatively low-resolution model, in which precipitation is calculated using the wind field gradient, and thus is subject to a greater error. A high-resolution model does indicate a consistently positive response of precipitation to obliquity maxima in latitudes higher than ~40°N (Chen et al., 2011). Nevertheless, the results are consistent with previous model experiments (Chen et al., 2011), which confirm a decreasing sea-level pressure over the Asian continent and an increasing high pressure over the surrounding oceans under maximal obliquity, and thus enhanced summer precipitation intensity caused by an increasing southerly wind because of the geostrophic balance (Fig. 1).

5. Conclusion

By extending the existing database, we show that microcodium Sr/Ca ratio is more reliable as a summer precipitation proxy on the Chinese Loess Plateau because of its weak dependence on temperature, calcification rate, and composition of the original soil solution compared with Mg/Ca ratio. The $\delta^{18}\text{O}$ values of Holocene microcodium indicate that microcodium is most likely crystallized during summer season and can therefore be used to reconstruct summer precipitation intensity. Two parallel records reconstructed

on the Chinese Loess Plateau covering the last 480 thousand years confirm the reliability of microcodium Sr/Ca proxy as a regional measure for summer precipitation. A dominant forcing by obliquity of summer precipitation is found before and after the mid-Pleistocene transition neither following the ice-volume-paced loess-paleosol sequences nor the speleothem records, suggesting that the loess-paleosol sequences and speleothem oxygen isotopic records are measures of other processes rather than the strength of EASM. Coupled with climate model results, we propose that the gradient of boreal insolation, which modulates the thermal contrast between the Asian continent and surrounding oceans, may play a significant role in regulating the strength of East Asia summer monsoon.

Acknowledgements

We wish to thank the editor (H.S.), Steven Clemens and two anonymous reviewers for their constructive comments. Support for this work comes from the National Natural Science Foundation of China funding (grant nos. 41230526, 41422205 and 41321062). This paper is ESMC Contribution No. 129.

Appendix A. Supplementary material

Supplementary material related to this article can be found online at <http://dx.doi.org/10.1016/j.epsl.2016.09.045>.

References

- An, Z., Clemens, S.C., Shen, J., Qiang, X., Jin, Z., Sun, Y., Prell, W.L., Luo, J., Wang, S., Xu, H., 2011. Glacial-interglacial Indian summer monsoon dynamics. *Science* 333, 719–723.
- An, Z., Kukla, G., Porter, S.C., Xiao, J., 1991. Late Quaternary dust flow on the Chinese loess plateau. *Catena* 18, 125–132.
- An, Z., Liu, T., Lu, Y., Porter, S.C., Kukla, G., Wu, X., Hua, Y., 1990. The long-term paleomonsoon variation recorded by the loess-paleosol sequence in Central China. *Quat. Int.* 7, 91–95.
- An, Z., Porter, S.C., Kutzbach, J.E., Xihao, W., Suming, W., Xiaodong, L., Xiaoqiang, L., Weijian, Z., 2000. Asynchronous Holocene optimum of the East Asian monsoon. *Quat. Sci. Rev.* 19, 743–762.
- Ao, H., Dekkers, M.J., Xiao, G., Yang, X., Qin, L., Liu, X., Qiang, X., Chang, H., Zhao, H., 2012. Different orbital rhythms in the Asian summer monsoon records from North and South China during the Pleistocene. *Glob. Planet. Change* 80–81, 51–60.
- Berger, A., Loutre, M.F., 1991. Insolation values for the climate of the last 10 million years. *Quat. Sci. Rev.* 10, 297–317.
- Böhm, F., Eisenhauer, A., Tang, J., Dietzel, M., Krabbenhöft, A., Kisakürek, B., Horn, C., 2012. Strontium isotope fractionation of planktic foraminifera and inorganic calcite. *Geochim. Cosmochim. Acta* 93, 300–314.
- Caley, T., Malaizé, B., Kageyama, M., Landais, A., Masson-Delmotte, V., 2013. Bihemispheric forcing for Indo-Asian monsoon during glacial terminations. *Quat. Sci. Rev.* 59, 1–4.
- Caley, T., Roche, D.M., Renssen, H., 2014. Orbital Asian summer monsoon dynamics revealed using an isotope-enabled global climate model. *Nat. Commun.* 5, 5371.
- Chen, F., Xu, Q., Chen, J., Birks, H.J., Liu, J., Zhang, S., Jin, L., An, C., Telford, R.J., Cao, X., Wang, Z., Zhang, X., Selvaraj, K., Lu, H., Li, Y., Zheng, Z., Wang, H., Zhou, A., Dong, G., Zhang, J., Huang, X., Bloemendal, J., Rao, Z., 2015. East Asian summer monsoon precipitation variability since the last deglaciation. *Sci. Rep.* 5, 11186.
- Chen, G.S., Liu, Z.Y., Clemens, S.C., Prell, W.L., Liu, X.D., 2011. Modeling the time-dependent response of the Asian summer monsoon to obliquity forcing in a coupled GCM: a PHASEMAP sensitivity experiment. *Clim. Dyn.* 36, 695–710.
- Chen, J., An, Z., Head, J., 1999. Variation of Rb/Sr ratios in the loess-paleosol sequences of Central China during the last 130,000 years and their implications for monsoon paleoclimatology. *Quat. Res.* 51, 215–219.
- Chen, J., Li, G., Yang, J., Rao, W., Lu, H., Balsam, W., Sun, Y., Ji, J., 2007. Nd and Sr isotopic characteristics of Chinese deserts: implications for the provenances of Asian dust. *Geochim. Cosmochim. Acta* 71, 3904–3914.
- Cheng, H., Edwards, R.L., Broecker, W.S., Denton, G.H., Kong, X., Wang, Y., Zhang, R., Wang, X., 2009. Ice age terminations. *Science* 326, 248–252.
- Cheng, H., Edwards, R.L., Sinha, A., Spötl, C., Yi, L., Chen, S., Kelly, M., Kathayat, G., Wang, X., Li, X., Kong, X., Wang, Y., Ning, Y., Zhang, H., 2016. The Asian monsoon over the past 640,000 years and ice age terminations. *Nature* 534, 640–646.
- Cheng, H., Sinha, A., Wang, X., Cruz, F.W., Edwards, R.L., 2012. The Global Paleomonsoon as seen through speleothem records from Asia and the Americas. *Clim. Dyn.* 39, 1045–1062.

- Clemens, S.C., Prell, W.L., Sun, Y., 2010. Orbital-scale timing and mechanisms driving Late Pleistocene Indo-Asian summer monsoons: reinterpreting cave speleothem $\delta^{18}\text{O}$. *Paleoceanography* 25.
- Ding, Y., Wang, Z., Sun, Y., 2008. Inter-decadal variation of the summer precipitation in East China and its association with decreasing Asian summer monsoon. Part I: observed evidences. *Int. J. Climatol.* 28, 1139–1161.
- Ding, Z.L., Liu, T.S., Rutter, N.W., Yu, Z.W., Guo, Z.T., Zhu, R.X., 1995. Ice-volume forcing of East-Asian winter monsoon variations in the past 800,000 years. *Quat. Res.* 44, 149–159.
- Eagle, R.A., Risi, C., Mitchell, J.L., Eiler, J.M., Seibt, U., Neelin, J.D., Li, G., Tripathi, A.K., 2013. High regional climate sensitivity over continental China constrained by glacial-recent changes in temperature and the hydrological cycle. *Proc. Natl. Acad. Sci.* 110, 8813–8818.
- Elderfield, H., Ferretti, P., Greaves, M., Crowhurst, S., McCave, I.N., Hodell, D., Piotrowski, A.M., 2012. Evolution of ocean temperature and ice volume through the mid-Pleistocene climate transition. *Science* 337, 704–709.
- Elderfield, H., Ganssen, G., 2000. Past temperature and $\delta^{18}\text{O}$ of surface ocean waters inferred from foraminiferal Mg/Ca ratios. *Nature* 405, 442–445.
- Fietzke, J., Eisenhauer, A., 2006. Determination of temperature-dependent stable strontium isotope ($^{88}\text{Sr}/^{86}\text{Sr}$) fractionation via bracketing standard MC-ICP-MS. *Geochem. Geophys. Geosyst.* 7, Q08009.
- Grinsted, A., Moore, J.C., Jevrejeva, S., 2004. Application of the cross wavelet transform and wavelet coherence to geophysical time series. *Nonlinear Process. Geophys.* 11, 561–566.
- Guo, Z.T., Ruddiman, W.F., Hao, Q.Z., Wu, H.B., Qiao, Y.S., Zhu, R.X., Peng, S.Z., Wei, J.J., Yuan, B.Y., Liu, T.S., 2002. Onset of Asian desertification by 22 Myr ago inferred from loess deposits in China. *Nature* 416, 159–163.
- Hao, Q., Wang, L., Oldfield, F., Peng, S., Qin, L., Song, Y., Xu, B., Qiao, Y., Bloemendal, J., Guo, Z., 2012. Delayed build-up of Arctic ice sheets during 400,000-year minima in insolation variability. *Nature* 490, 393–396.
- Huybers, P., Tziperman, E., 2008. Integrated summer insolation forcing and 40,000-year glacial cycles: the perspective from an ice-sheet/energy-balance model. *Paleoceanography* 23.
- Kim, S.-T., O'Neil, J.R., 1997. Equilibrium and nonequilibrium oxygen isotope effects in synthetic carbonates. *Geochim. Cosmochim. Acta* 61, 3461–3475.
- Li, G., Chen, J., Chen, Y., Yang, J., Ji, J., Liu, L., 2007a. Dolomite as a tracer for the source regions of Asian dust. *J. Geophys. Res.* 112, D17201. <http://dx.doi.org/10.1029/2007JD008676>.
- Li, G., Chen, J., Ji, J., Yang, J., Conway, T.M., 2009. Natural and anthropogenic sources of East Asian dust. *Geology* 37, 727–730.
- Li, G., Sheng, X., Chen, J., Yang, J., Chen, Y., 2007b. Oxygen-isotope record of paleorainwater in authigenic carbonates of Chinese loess-paleosol sequences and its paleoclimatic significance. *Palaeogeogr. Palaeoclimatol. Palaeoecol.* 245, 551–559.
- Li, T., Li, G., 2014. Incorporation of trace metals into microcodium as novel proxies for paleo-precipitation. *Earth Planet. Sci. Lett.* 386, 34–40.
- Lisiecki, L.E., Raymo, M.E., 2005. A Pliocene–Pleistocene stack of 57 globally distributed benthic $\delta^{18}\text{O}$ records. *Paleoceanography* 20, PA1003. <http://dx.doi.org/10.1029/2004PA001071>.
- Liu, H.-C., You, C.-F., Huang, K.-F., Chung, C.-H., 2012. Precise determination of triple Sr isotopes ($\delta^{87}\text{Sr}$ and $\delta^{88}\text{Sr}$) using MC-ICP-MS. *Talanta* 88, 338–344.
- Liu, T., Ding, Z., 1998. Chinese loess and the paleomonsoon. *Annu. Rev. Earth Planet. Sci.* 26, 111–145.
- Liu, W., Huang, Y., An, Z., Clemens, S.C., Li, L., Prell, W.L., Ning, Y., 2005. Summer monsoon intensity controls C4/C3 plant abundance during the last 35 ka in the Chinese Loess Plateau: carbon isotope evidence from bulk organic matter and individual leaf waxes. *Palaeogeogr. Palaeoclimatol. Palaeoecol.* 220, 243–254.
- Liu, Z., Wen, X., Brady, E.C., Otto-Bliessner, B., Yu, G., Lu, H., Cheng, H., Wang, Y., Zheng, W., Ding, Y., Edwards, R.L., Cheng, J., Liu, W., Yang, H., 2014. Chinese cave records and the East Asia Summer Monsoon. *Quat. Sci. Rev.* 83, 115–128.
- Lu, H., Yi, S., Liu, Z., Mason, J.A., Jiang, D., Cheng, J., Stevens, T., Xu, Z., Zhang, E., Jin, L., 2013. Variation of East Asian monsoon precipitation during the past 21 ky and potential CO_2 forcing. *Geology* 41, 1023–1026.
- Maher, B.A., Thompson, R., 2012. Oxygen isotopes from Chinese caves: records not of monsoon rainfall but of circulation regime. *J. Quat. Sci.* 27, 615–624.
- Mavromatis, V., Gautier, Q., Bosc, O., Schott, J., 2013. Kinetics of Mg partition and Mg stable isotope fractionation during its incorporation in calcite. *Geochim. Cosmochim. Acta* 114, 188–203.
- Orland, I.J., Edwards, R.L., Cheng, H., Kozdon, R., Cross, M., Valley, J.W., 2015. Direct measurements of deglacial carbon strength in a Chinese stalagmite. *Geology* 43, 555–558.
- Peterse, F., Martínez-García, A., Zhou, B., Beets, C.J., Prins, M.A., Zheng, H., Eglinton, T.I., 2014. Molecular records of continental air temperature and monsoon precipitation variability in East Asia spanning the past 130,000 years. *Quat. Sci. Rev.* 83, 76–82.
- Petit, J.R., Jouzel, J., Raynaud, D., Barkov, N.I., Barnola, J.M., Basile, I., Bender, M., Chappellaz, J., Davis, M., Delaygue, G., Delmotte, M., Kotlyakov, V.M., Legrand, M., Lipenkov, V.Y., Lorius, C., Pepin, L., Ritz, C., Saltzman, E., Stievenard, M., 1999. Climate and atmospheric history of the past 420,000 years from the Vostok ice core, Antarctica. *Nature* 399, 429–436.
- Prins, M.A., Vriend, M., Nugteren, G., Vandenbergh, J., Lu, H., Zheng, H., Jan Weltje, G., 2007. Late Quaternary aeolian dust input variability on the Chinese Loess Plateau: inferences from unmixing of loess grain-size records. *Quat. Sci. Rev.* 26, 230–242.
- Quade, J., Eiler, J., Daëron, M., Achyuthan, H., 2013. The clumped isotope geothermometer in soil and paleosol carbonate. *Geochim. Cosmochim. Acta* 105, 92–107.
- Rao, W., Chen, J., Yang, J., Ji, J., Zhang, G., 2009. Sr isotopic and elemental characteristics of calcites in the Chinese deserts: implications for eolian Sr transport and seawater Sr evolution. *Geochim. Cosmochim. Acta* 73, 5600–5618.
- Rao, Z., Jia, G., Li, Y., Chen, J., Xu, Q., Chen, F., 2016. Asynchronous evolution of the isotopic composition and amount of precipitation in north China during the Holocene revealed by a record of compound-specific carbon and hydrogen isotopes of long-chain n-alkanes from an alpine lake. *Earth Planet. Sci. Lett.* 446, 68–76.
- Raymo, M.E., Lisiecki, L.E., Nisancioglu, K.H., 2006. Plio-Pleistocene Ice volume, Antarctic climate, and the global $\delta^{18}\text{O}$ record. *Science* 313, 492–495.
- Rosenbloom, N.A., Otto-Bliessner, B.L., Brady, E.C., Lawrence, P.J., 2013. Simulating the mid-Pliocene Warm Period with the CCSM4 model. *Geosci. Model Dev.* 6, 549–561.
- Sheng, X., Chen, J., Ji, J., Chen, T., Li, G., Teng, H.H., 2008. Morphological characters and multi-element isotopic signatures of carbonates from Chinese loess-paleosol sequences. *Geochim. Cosmochim. Acta* 72, 4323–4337.
- Sun, D., An, Z., Shaw, J., Bloemendal, J., Sun, Y., 1998. Magnetostratigraphy and paleoclimatic significance of Late Tertiary aeolian sequences in the Chinese Loess Plateau. *Geophys. J. Int.* 134, 207–212.
- Sun, Y., Clemens, S.C., An, Z., Yu, Z., 2006. Astronomical timescale and palaeoclimatic implication of stacked 3.6-Myr monsoon records from the Chinese Loess Plateau. *Quat. Sci. Rev.* 25, 33–48.
- Tang, J., Köhler, S.J., Dietzel, M., 2008. $\text{Sr}^{2+}/\text{Ca}^{2+}$ and $^{44}\text{Ca}/^{40}\text{Ca}$ fractionation during inorganic calcite formation: I. Sr incorporation. *Geochim. Cosmochim. Acta* 72, 3718–3732.
- Thomas, E.K., Clemens, S.C., Prell, W.L., Herbert, T.D., Huang, Y., Liu, Z., Sinninghe Damste, J.S., Sun, Y., Wen, X., 2014. Temperature and leaf wax ^2H records demonstrate seasonal and regional controls on Asian monsoon proxies. *Geology* 42, 1075–1078.
- Thomas, E.K., Clemens, S.C., Sun, Y., Prell, W.L., Huang, Y., Gao, L., Loomis, S., Chen, G., Liu, Z., 2016. Heterodynes dominate precipitation isotopes in the East Asian monsoon region, reflecting interaction of multiple climate factors. *Earth Planet. Sci. Lett.* 455, 196–206.
- Torrence, C., Compo, G.P., 1998. A practical guide to wavelet analysis. *Bull. Am. Meteorol. Soc.* 79, 61–78.
- Wang, B., Liu, J., Kim, H.-J., Webster, P., Yim, S.-Y., 2012. Recent change of the global monsoon precipitation (1979–2008). *Clim. Dyn.* 39, 1123–1135.
- Wang, Y., Cheng, H., Edwards, R.L., He, Y., Kong, X., An, Z., Wu, J., Kelly, M.J., Dykoski, C.A., Li, X., 2005. The Holocene Asian monsoon: links to Solar changes and North Atlantic climate. *Science* 308, 854–857.
- Wang, Y., Cheng, H., Edwards, R.L., Kong, X., Shao, X., Chen, S., Wu, J., Jiang, X., Wang, X., An, Z., 2008. Millennial- and orbital-scale changes in the East Asian monsoon over the past 224,000 years. *Nature* 451, 1090–1093.
- Yancheva, G., Nowaczyk, N.R., Mingram, J., Dulski, P., Schettler, G., Negendank, J.F., Liu, J., Sigman, D.M., Peterson, L.C., Haug, G.H., 2007. Influence of the intertropical convergence zone on the East Asian monsoon. *Nature* 445, 74–77.
- Yuan, D., Cheng, H., Edwards, R.L., Dykoski, C.A., Kelly, M.J., Zhang, M., Qing, J., Lin, Y., Wang, Y., Wu, J., Dorale, J.A., An, Z., Cai, Y., 2004. Timing, duration, and transitions of the last interglacial Asian Monsoon. *Science* 304, 575–578.
- Zhang, X., Yao, T., 1998. Distributional features of $\delta^{18}\text{O}$ in precipitation in China. *Acta Geogr. Sin.* 53, 70–78 (in Chinese with English abstracts).
- Zhou, L.P., Oldfield, F., Wintle, A.G., Robinson, S.G., Wang, J.T., 1990. Partly pedogenic origin of magnetic variations in Chinese loess. *Nature* 346, 737–739.
- Zhou, W., Warren Beck, J., Kong, X., An, Z., Qiang, X., Wu, Z., Xian, F., Ao, H., 2014. Timing of the Brunhes–Matuyama magnetic polarity reversal in Chinese loess using ^{10}Be . *Geology* 42, 467–470.